

# Measurement of the Transition Temperature Governing the Photoinduced Reversible Solid-to-Liquid Transition of Azobenzene-Containing Polymers

David Siniscalco, Laurence Pessoni, Laurent Billon, Anne Boussonnière, Anne-Sophie Castanet, Jean-François Bardeau, Pierre Nickmilder, Philippe Leclère, and Nicolas Delorme\*



Cite This: *ACS Appl. Polym. Mater.* 2023, 5, 7358–7363



Read Online

ACCESS |



Metrics & More



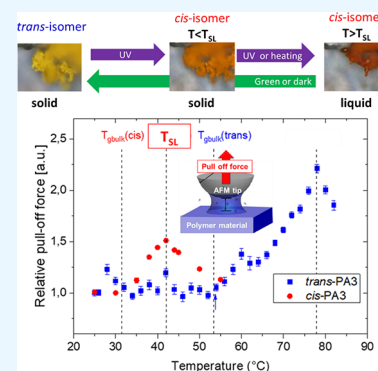
Article Recommendations



Supporting Information

**ABSTRACT:** The ability to observe photoinduced reversible solid-to-liquid transitions for some polymers bearing photo-active azobenzene groups (azopolymers) has become a competitive research field in materials science and technology because of their potential applications in photocontrolled adhesives, photohealable materials, or soft lithography. Unfortunately, methods to accurately characterize this transition are scarce and mainly qualitative, which limits the understanding of the parameters governing it. In the first part of this paper, we will show that the photoinduced reversible solid-to-liquid transition can be associated to a transition temperature (named  $T_{SL}$ ). This transition temperature can be accurately measured using a scanning probe microscopy-based method. Then, the measurement of  $T_{SL}$  on azopolymers with different chemical structures will allow us to understand why the experimental irradiation conditions to observe the solid-to-liquid transition were different. With the possibility to accurately characterize the photoinduced solid-to-liquid transition, we believe that this work paves the way to the optimization of azopolymer design for a better photocontrol of their mechanical properties.

**KEYWORDS:** azobenzene, photoreversible solid-to-liquid transition, azopolymer, AFM, force spectroscopy, nano-dynamic mechanical analysis



## INTRODUCTION

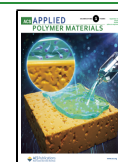
Despite their first synthesis in 1834, it was only in 1937 that Hartley first reported the reversible *trans* (*E*) to *cis* (*Z*) photoisomerization of azobenzene molecules. Since then, azobenzene molecules have been associated with a multitude of materials to control their properties by light.<sup>1</sup> The photoresponsive characteristics of azomolecule-containing polymers (azopolymers) and their subsequent applications have been intensively studied in the past decades.<sup>2,3</sup> Among them, since its first mention in 2017,<sup>4</sup> the ability to observe a photoreversible solid-to-liquid transition has become a competitive research field in materials science and technology because of its potential applications in photocontrolled adhesives,<sup>3,5</sup> photohealable materials,<sup>4</sup> or soft lithography.<sup>6</sup> Despite numerous publications on the application of the photoreversible solid-to-liquid transitions, to our knowledge, the only proposed mechanism hypothesizes that the photoreversible solid-to-liquid transition is due to a glass temperature variation during the *trans*-to-*cis* photoisomerization.<sup>7</sup> The transition may occur when the temperature of the azopolymer is between the glass transition temperature (*i.e.*,  $T_g$ ) of the *cis* form and that of the *trans* one.<sup>7</sup> This hypothesis is widely used<sup>1,3,8,9</sup> to explain the properties of azopolymers exhibiting a reversible phase transition. However, since  $T_g$  is known to be a

transition between a vitreous and a viscoelastic state, it seems probable that  $T_g$  *cis* or *trans* is not the real transition temperature governing the solid-to-liquid transition. As a consequence, it is still unclear how the isomerization of azobenzene is coupled with the chain dynamics of azopolymers, which is critical for applications like the photoinduced solid-to-liquid transition.<sup>10</sup> The lack of study probably lies in the fact that the detection of this transition is made in almost all situations in a qualitative way. Indeed, for bulk materials, optical microscopy is usually used.<sup>3,6,11</sup> Although easy to set up, this method is not satisfactory if one wants to accurately determine the transition conditions. Indeed, the “appearance” of droplets under the microscope depends on the objective magnification, the size of the material grain, etc. In addition, the obtained transition time depends on the illumination conditions (*i.e.*, light intensity).<sup>12</sup>

Received: June 12, 2023

Accepted: July 31, 2023

Published: August 8, 2023



Differential scanning calorimetry (DSC) is the technique of choice for measuring transitions in polymeric materials. Its use for azopolymers allows the measurements of glass transition temperature, *cis*-to-*trans* isomerization, and liquid crystalline phase transitions for both *trans* and *cis* isomers.<sup>4</sup> However, to our knowledge, the solid-to-liquid transition was never detected with this technique. Dynamic mechanical analysis (DMA) has been used to study the viscoelastic properties of azopolymers. Zhang *et al.* mentioned a flow temperature ( $T_f$ ) “a few degrees higher than the  $T_g$ ” but no direct relationship was made with the solid-to-liquid transition and the way to determine the value of this flow temperature is imprecise.<sup>11</sup> For many applications such as photohealable coating, reversible adhesive..., the azopolymer has to be used as a coating, but all the abovementioned techniques are not applicable due to the small quantity of available material.

To accurately detect the solid-to-liquid transition of azopolymer coatings, we have developed a new method based on atomic force microscopy (AFM). This method consists in measuring the force needed to detach an AFM tip from the film surface after a contact with a controlled load (*i.e.*, pull-off force). The pull-off force is known to be influenced by the wetting properties of the polymer surface and the polymer viscoelastic properties.<sup>13</sup> We have shown in the past that when performed as a function of the sample temperature, the measurement of the pull-off force allowed the detection of subtle thermomechanical transition in polymer materials such as surface or bulk glass transition temperature and even for polymer thin films with thicknesses down to 7 nm.<sup>14</sup> In this work, we will demonstrate that the solid-to-liquid transition can be associated to a transition temperature called solid-to-liquid temperature ( $T_{SL}$ ) that can be, for the first time, effectively measured. We also used AFM in the recently nano-dynamic mechanical analysis (nano-DMA) mode to quantify the viscoelastic properties of the studied thin films (see below).

## EXPERIMENTAL SECTION

**Azopolymer Synthesis.** The chemical formula and properties of the two azopolymers (PA3 and PB1) used in this study are presented in Table 1. The azopolymers were synthesized using nitroxide-mediated polymerization (NMP) following the procedure described by Pessoni *et al.*<sup>12</sup> The molecular weight and dispersity values of polymers were measured using size exclusion chromatography (SEC)

**Table 1. Chemical Structures and Properties of the PA3 and PB1 Azopolymers**

Azopolymer name	PA3	PB1
Formula		
$M_n$ (g/mol) <sup>a</sup> / $T_{g,trans}$ (°C) <sup>b</sup>	5900 / 55	6000 / 54

<sup>a</sup>Measured by SEC. <sup>b</sup>Measured by DSC.

using THF as an eluent. Number-average molar mass ( $M_n$ ) values of the polymers were calculated from a calibration derived from polystyrene standards.

**Azopolymer Coatings.** Azopolymer thin films were prepared on UV-ozone cleaned microscopic glass slides by drop casting a solution of the azopolymer in  $\text{CH}_2\text{Cl}_2$  ( $C = 10 \text{ g/L}$ ). The films were then dried under vacuum for 24 h. The resulting film thicknesses, measured by AFM after performing a scratch on the film, were close to 1.5  $\mu\text{m}$ .

**Differential Scanning Calorimetry.** Glass transition temperature ( $T_g$ ) and nematic-to-isotropic liquid crystalline transition ( $T_{NI}$ ) were measured using a Differential Scanning Calorimetry (DSC) TA Instrument at  $10 \text{ }^\circ\text{C}\cdot\text{min}^{-1}$ . Two cycles of temperature containing a heating part, from  $-30$  to  $150 \text{ }^\circ\text{C}$ , and a cooling one to  $-30 \text{ }^\circ\text{C}$  were realized. The value of the  $T_g$  of the second cycle was chosen for the  $T_g$  of the *trans* isomer. DSC analysis on *cis* isomers was performed following the method described by Zhou *et al.*<sup>4</sup> *Trans* isomers were dissolved in  $\text{CH}_2\text{Cl}_2$  and then illuminated with UV light under stirring. The solvent was removed under vacuum. <sup>1</sup>H NMR analysis of the photoisomerization in  $\text{CD}_2\text{Cl}_2$  under the same irradiation conditions indicated *trans*-to-*cis* conversion rates above 73%. *Cis* isomers were finally studied by DSC between  $-30$  and  $70 \text{ }^\circ\text{C}$  at  $20 \text{ }^\circ\text{C}\cdot\text{min}^{-1}$ . TRIOS software version 5.0. was used for DSC treatment.

**Atomic Force Microscopy (AFM).** All force–distance AFM measurements were performed with an Agilent 5500 AFM equipped with an environmental chamber. Temperature control was monitored by a PID controller (Lakeshore) connected to a heat stage allowing heating from  $T = 20$  to  $250 \text{ }^\circ\text{C}$  with an accuracy of  $0.1 \text{ }^\circ\text{C}$ . The controller was calibrated with standard fusion point solids (azobenzene ( $T_f = 68 \text{ }^\circ\text{C}$ ) and acetanilide ( $T_f = 114.5 \text{ }^\circ\text{C}$ )). Force–distance curves were recorded using the same CP-FM-SiO-B tip equipped with a silica sphere ( $R = 3.5 \mu\text{m}$ ) with a spring constant of  $0.92 \text{ N}\cdot\text{m}^{-1}$  (measured by the thermal noise method).<sup>15</sup> A calibrated z-close loop scanner was used to carefully control the indentation depth, and a maximum load (100 nN) was fixed to prevent any critical indentation of the film. All the force–distance curves were conducted at 1 Hz. Pull-off force values were measured from the retraction force–distance curve as the difference between the minimum force and the force at large distances.<sup>14</sup> For each temperature, a  $4 \times 4$  pixel mapping on a  $2 \times 2 \mu\text{m}^2$  surface (with each pixel containing 10 force–distance curves) was averaged to give the pull-off force intensities and uncertainties. Picoview software from Agilent and Atomic J freeware version 2.0<sup>16</sup> were used to analyze and extract pull-off forces and Young’s moduli (JKR model, Poisson ratio = 0.33).

**Nano-Dynamic Mechanical Analysis.** AFM nano-DMA is a recently developed AFM mode to quantify the viscoelastic properties at the nanoscale.<sup>17</sup> It has been performed on a wide range of samples, from biological samples to heterogenous nanocomposites. The “measurement process” is similar to force–distance curve measurement, except that when the tip is in contact with the studied sample, the load is maintained and a frequency modulation is applied to the tip.<sup>18</sup> The difference of phase between the dynamic solicitation and the cantilever deflection, coupled with the force–curves analysis, gives access to local rheological parameters of the sample, such as storage modulus ( $E'$ ), loss modulus ( $E''$ ), and damping factor ( $\tan \delta$ ).

AFM nano-DMA has two modes. The first is an imaging mode where the frequency modulation is fixed and the tip scans the surface, providing quantitative mapping of viscoelastic properties. The second is a spectroscopic mode where the position of the tip is fixed while a ramp script of discrete frequencies is applied, providing the evolution of rheological properties as a function of those frequencies.

All nano-DMA measurements were performed on a Dimension Icon AFM (Bruker Corp.). Temperature control was monitored by a PID controller (Lakeshore) connected to a heat stage inside the AFM device. The probes used are pre-calibrated RTESPA 300-30 cantilevers from Bruker Corp. with a spring constant around  $40 \text{ Nm}^{-1}$  and a tip radius of 30 nm.

All measurements were done in spectroscopic mode with frequencies randomly chosen within the range from 1 to 160 Hz. For each temperature, a series of  $3 \times 3$  grid acquisitions over a  $1 \mu\text{m}^2$

area were collected. The homogeneity in terms of morphology and mechanical properties (adhesion, Young's modulus, and indentation) of those areas were previously checked by peak force tapping mode. Nanoscope Analysis 3.0 was used to analyze and extract data.

## RESULTS AND DISCUSSION

Figure 1 shows the evolution of the normalized pull-off force (*i.e.*, pull-off force measured at temperature  $T$  divided by pull-

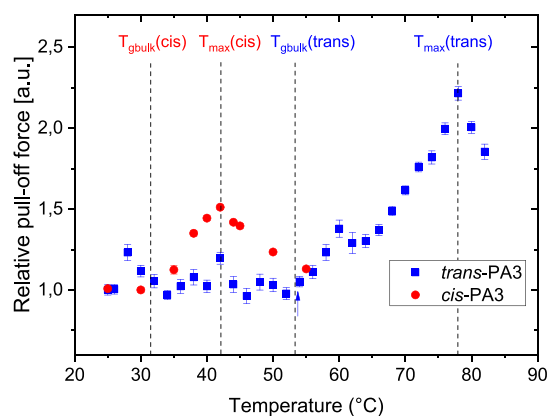


**Figure 1.** Evolution of the normalized pull-off force as a function of temperature for the PA3 azopolymer before (*trans*-PA3) and after UV irradiation (*cis*-PA3) ( $\lambda_{\text{max}} = 365 \text{ nm}$ ,  $E_e = 300 \text{ mW}\cdot\text{cm}^{-2}$ ,  $T = 30 \text{ s}$ ).

off force at  $T = 25 \text{ }^\circ\text{C}$ ) with temperature for the PA3 film before (*trans*-PA3) and after UV irradiation (*cis*-PA3). For *trans*-PA3, we observe for  $T < 50 \text{ }^\circ\text{C}$  a domain where the pull-off force remains almost constant, indicating no major change of the adhesion properties. From  $T = 55 \text{ }^\circ\text{C}$ , an increase in the pull-off force is observed until a maximum value is reached for  $T_{\text{max}} = 78 \text{ }^\circ\text{C}$ . After this point, the pull-off force decreases progressively. Based on our previous study,<sup>14</sup> the transition temperature between 50 and 55  $^\circ\text{C}$  can be associated with the glass temperature ( $T_g$ ) of the *trans*-PA3, which was confirmed by DSC on the bulk polymer (Figure S1). When a similar experiment is performed on *cis*-PA3, the pull-off force vs temperature curve is translated toward lower temperatures. Indeed,  $T_g$  *cis* is measured between 30 and 35  $^\circ\text{C}$  and the temperature of maximum pull-off force is measured at  $T_{\text{max}} = 42 \text{ }^\circ\text{C}$ , which is also confirmed by a small decrease in the heat flow on the DSC chart (Figure S1). The reversibility of the process is demonstrated by performing the *cis* to *trans* back isomerization (*i.e.*, irradiating the *cis*-PA3 with green light or keeping in the dark for 24 h) and by obtaining a pull-off vs temperature curve similar to that of the *trans*-PA3 (Figure S2).

During the pull-off force measurement, the Young's modulus can also be measured. Figure 2 shows the evolution of the Young's modulus with temperature for both *trans*- and *cis*-PA3. Figure 2 is similar to those already observed for azopolymers.<sup>11</sup> At room temperature, both isomers have a modulus close to 0.1 GPa, characteristic of the hard glassy behavior of a polymer with low molecular mass ( $M_n$ ). As expected, increasing the temperature close to the  $T_g$  of the polymer led to a decrease in the Young's modulus. Only for *trans*-PA3 that a short rubber plateau, typical of polymers with entangled or cross-linked chains, can be observed between  $T = 57 \text{ }^\circ\text{C}$  and  $T = 64 \text{ }^\circ\text{C}$ . Since the theoretical critical entanglement molecular weight of PA3 ( $M_c = 68 \text{ kDa}$ )<sup>19</sup> is much higher than its  $M_n$  (5.9 kDa), there is no chain entanglement for PA3.

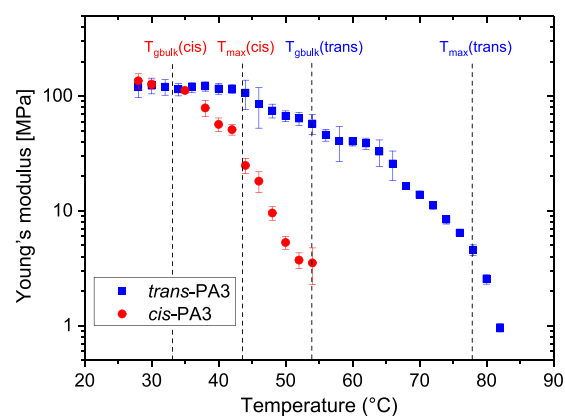


**Figure 2.** Evolution of the Young's modulus as a function of temperature for the PA3 azopolymer before (*trans*-PA3) and after UV irradiation (*cis*-PA3) ( $\lambda_{\text{max}} = 365 \text{ nm}$ ,  $E_e = 300 \text{ mW}\cdot\text{cm}^{-2}$ ,  $t = 30 \text{ s}$ ).

Consequently, the presence of a plateau may reflect the existence of strong interchain interactions for this temperature range. For both polymers, the measured  $T_{\text{max}}$  by the pull-off force experiment is not clearly visible on the Young's modulus versus temperature curve, indicating that the temperature of maximum adhesion is probably fairly little linked to the elastic properties of the polymer.

The presence of a maximum in the pull-off force vs temperature curve was already observed by our team for thin PS films.<sup>14</sup> Kim *et al.* also detected this maximum for PMMA using a tribometer<sup>20</sup> when undulations, known as Saffman–Taylor instabilities,<sup>21</sup> formed at the periphery of the contact between the rigid probe and the polymer material. The occurrence of Saffman–Taylor instabilities indicates that the polymer material is in a viscous flow state in this temperature range.<sup>22</sup> The shape of the force–distance curves (Figure 3) obtained by AFM below and above  $T_{\text{max}}$  for *trans*-PA3 confirms the change in the mechanical properties of the material at  $T_{\text{max}}$ . Indeed, in contrast to the force–distance curves obtained at  $T = 65 \text{ }^\circ\text{C}$ , a high hysteresis between the approach and retraction curves, a high pull-off force, and a high separation distance ( $D$ ) (*i.e.*, the distance between the point of maximum adhesion and the full detachment of the AFM tip) are observed for  $T = 80 \text{ }^\circ\text{C}$ . These changes are characteristic of a transition between an elastic behavior and a behavior where energy dissipation is intense, confirming the appearance of a viscous behavior at  $T > T_{\text{max}}$ . For *cis*-PA3, the change of behavior at  $T > T_{\text{max}}$  is subtler, but it is clearly observable with the increase in  $D$  and the rounder shape of the retraction curve.

To confirm the viscoelastic nature of the transition observed at  $T_{\text{max}}$  we performed nano-DMA measurements. This recent SPM-based technique<sup>17</sup> makes it possible, by oscillating the sample at a given frequency, to access both the storage modulus ( $E'$ ) and loss modulus ( $E''$ ) as a function of frequency or temperature. The measurements carried out on *trans*- and *cis*-PA3 show a decrease in both  $E'$  and  $E''$  with temperature (Figure S3) as expected for low mass polymers.<sup>23</sup>  $\tan \delta$  is commonly referred to as the loss factor and conveniently describes the viscoelastic behavior of the material as a ratio between the energy loss and stored during deformation (*i.e.*,  $E''/E'$ ). Figure 4 shows the evolution of  $\tan \delta$  for *trans*- and *cis*-PA3 as a function of temperature and for three different frequencies. For *trans*-PA3, if a very slight maximum at  $T = 50 \text{ }^\circ\text{C}$  (close to  $T_g$ ) is only observable at a low frequency (*i.e.*, 1



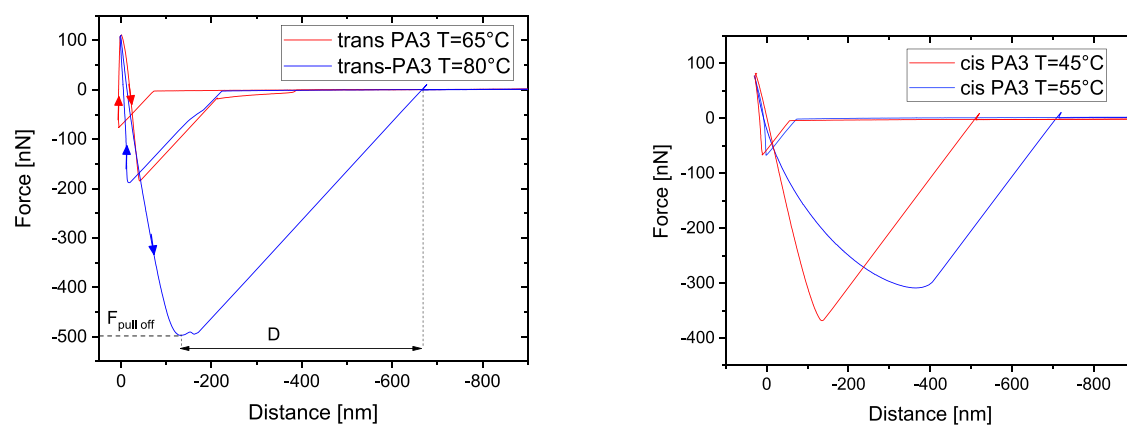


**Figure 3.** Approach and retraction force–distance curves obtained for the *trans*-PA3 and *cis*-PA3 below and above their respective  $T_{\max}$ . On the *trans*-PA3,  $F_{\text{pull-off}}$  and  $D$  indicate, respectively, the intensity of the pull-off force and the distance needed to detach the AFM tip from the surface.

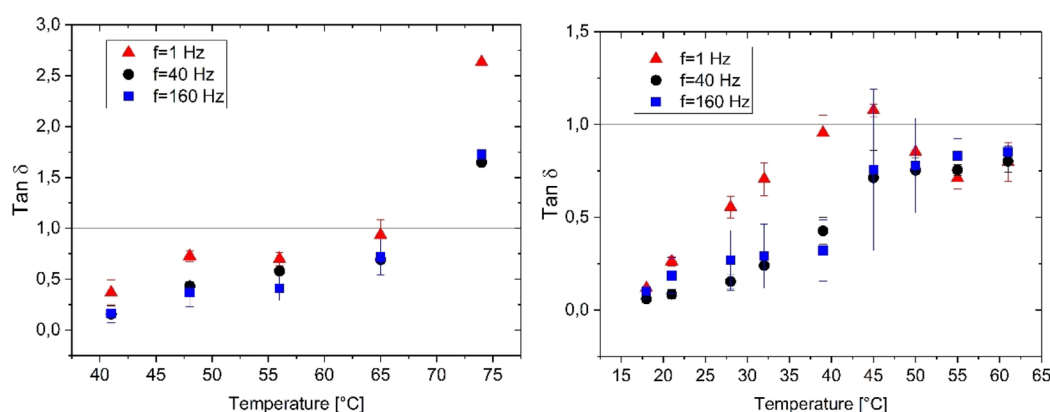


**Figure 4.** Evolution of  $\tan \delta$  with temperature for *trans*-PA3 (left) and *cis*-PA3 (right) measured by nano-DMA for three frequencies.

Hz), a strong increase in  $\tan \delta$  up to the temperature of 75 °C (close to  $T_{\max}$ ) is observed for all frequencies. The strong increase in  $\tan \delta$  is characteristic of strong dissipation and confirms the viscous character of the material at a temperature very close to  $T_{\max}$ . Unfortunately, for higher temperatures, the tip–sample interaction was too strong to allow the measurement of the mechanical properties. For *cis*-PA3, no maximum is clearly detected at the temperature corresponding to the  $T_g$  (*cis*) but a maximum is observed at a low frequency for  $T = T_{\max}$ . Again, the viscous character of the transition observed at  $T_{\max}$  is confirmed. The  $\tan \delta$  peak at  $T_{\max}$  is only visible for frequencies below 50 Hz (Figure 4), which may indicate that the characteristic time of the transition is close above 0.2 ms. Even if the understanding of the link between measurement of pull-off force and measurement of  $\tan \delta$  is beyond the scope of this article, it is interesting to notice the similarity in the shapes of the  $\tan \delta$  curves (*trans*- and *cis*-PA3) obtained with both techniques at a frequency of 1 Hz.

With these results, we can now assert with confidence that the temperature where the maximum pull-off force is detected ( $T_{\max}$ ) for both *trans* and *cis* isomers can be associated to a solid-like to liquid-like transition temperature.

To link the measured  $T_{\max}$  and the photoinduced solid-to-liquid transition observed in azopolymers, we made an experiment consisting in observing under a microscope small grains (average diameter = 20  $\mu\text{m}$ ) of PA3 (Figure 5). At room temperature, without irradiation, pristine yellow solid grains (*trans*-PA3) can be observed. Then, the sample was irradiated on a Peltier stage to keep the sample temperature at 25 °C. As

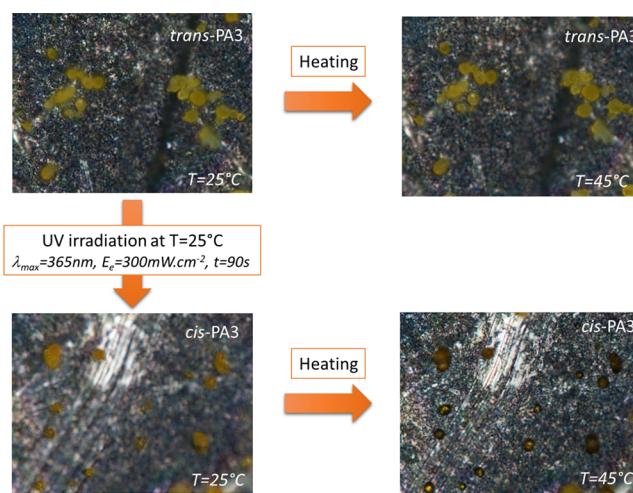


**Figure 5.** Optical microscopy pictures (350  $\times$  264  $\mu\text{m}$ ) of PA3 grains as a function of substrate temperature for *trans*-PA3 and *cis*-PA3.

shown on Figure 5, a change of color (yellow to orange) characteristic of the *trans*-to-*cis* isomerization is observed but the grains remain solid. The solid-to-liquid phase transition is only observed when the grains are heated above  $T = T_{\max}(\textit{cis}) = 42$  °C.

Our results clearly demonstrate that the reversible photoinduced solid-to-liquid transition interesting for numerous applications can be associated to a transition temperature named  $T_{\text{SL}}$  that can be measured by AFM as the maximum of

the pull-off force vs temperature curve of the *cis* isomer ( $=T_{\max}^{\text{cis}}$ ).

Now that we have an accurate method to detect the photoinduced solid-to-liquid transition, we can compare different azopolymers to understand which parameters may influence this transition. We have studied another azopolymer (named PB1) with a similar  $M_n$  (6000 g/mol) but with a different chemical composition (Table 1). For PB1, whereas the same para-substituent ( $-\text{CH}_3$ ) of the azobenzene group is present, the linker chain possesses a longer length than PA3 ( $\text{C}_{10}\text{H}_{20}$  for PB1 and  $\text{C}_6\text{H}_{12}$  for PA3). AFM pull-off force vs temperature was performed on both *trans*- and *cis*-PB1 (Figure S4), and transition temperatures were extracted from these curves (Table 2).

**Table 2. Transition Temperatures (in °C) Measured by AFM for PA3 and PB1 Azopolymers**

	PA3		PB1	
	<i>trans</i>	<i>cis</i>	<i>trans</i>	<i>cis</i>
$T_g$	52 (2)	32 (2)	55 (2)	0 (2)
$T_{\max}$	78 (2)	42 (2) = $T_{\text{SL}}$	70 (2)	15 (2) = $T_{\text{SL}}$

On the one hand, PA3 and PB1 show similar  $T_g$  and  $T_{\max}$  values for the *trans* isomers. On the other hand, a decrease of 30 °C is observed for both  $T_g^{\text{cis}}$  and  $T_{\max}^{\text{cis}}$  (i.e.,  $T_{\text{SL}}$ ) between PA3 and PB1. These results may indicate that like  $T_g$ , the  $T_{\text{SL}}$  is influenced by the polymer chain dynamics. The decrease in these two temperatures may be explained by the presence of a longer and therefore more flexible linker for PB1, which facilitates the movements of the polymer chains. This effect seems to be more important for the *cis* form than for the *trans* for which the transition temperatures have similar values. These differences probably lie in the fact that the bent *cis*-azomolecule impacts the dynamics of the chains more than the *trans* with its rod-like shape.

The comparison of the two polymers properties allows us to better understand why, despite comparable *trans*-to-*cis* isomerization kinetics,<sup>24</sup> the PA3 photoinduced solid-to-liquid transition needed a longer irradiation duration (45 s against 30 s at 365 nm and 340 mW·cm<sup>-2</sup>) than PB1 to be observable. Indeed, under UV irradiation, the *trans*-to-*cis* isomerization leads to a modification of the thermomechanical properties of the azopolymer, characterized by a reduction of both  $T_g$  and  $T_{\max}$ . We have seen previously that the photoinduced solid-to-liquid transition occurs only if the sample temperature is above  $T_{\text{SL}}$  ( $T_{\max}^{\text{cis}}$ ). Since the  $T_{\text{SL}}$  of PB1 is lower than the  $T_{\text{SL}}$  of PA3 (Table 1), the  $T_{\text{SL}}$  of the PA3 sample is reached by increasing the irradiation time. As shown for PA3 on Figure 5, this temperature may have been reached with the same irradiation time of PB1 but with the help of an external heating source. The difference in irradiation duration to reach the photoinduced solid-to-liquid transition can now be simply explained by the difference in  $T_{\text{SL}}$  value.

## CONCLUSIONS

In this work, we have demonstrated that measurement by AFM of the pull-off force vs temperature is an effective way to detect the photoinduced solid-to-liquid transition of azopolymers. Indeed, we have shown that this transition occurs at a temperature called  $T_{\text{SL}}$  corresponding to the temperature

where the pull-off force on the *cis*-azopolymer reaches a maximum value.

By comparing two azopolymers with azobenzene groups with different chemical natures, we have shown that the difference in irradiation duration needed to observe the solid-to-liquid transition can be explained by a difference in  $T_{\text{SL}}$ . With the possibility to accurately characterize the photoinduced solid-to-liquid transition, we believe that the opportunity is given to the community to study the physical parameters (chemical structure, polymer backbone...) that can influence this transition and thus to be able to design polymers with a  $T_{\text{SL}}$  compatible with the application domain (i.e., photohealable material, photoreversible adhesive...). The influence of the azopolymer molecular weight and the chemical structure of the azo group on the values of  $T_g$  and  $T_{\text{SL}}$  will be presented in an upcoming paper.

## ASSOCIATED CONTENT

### Supporting Information

The Supporting Information is available free of charge at <https://pubs.acs.org/doi/10.1021/acscapm.3c01256>.

DSC charts of the PA3-azopolymer, demonstration of the reversibility of the pull-off force vs temperature measurements, evolution of  $E'$  and  $E''$  measured by nano-DMA, and evolution of the normalized pull-off force as a function of temperature for PB1-azopolymer (PDF)

## AUTHOR INFORMATION

### Corresponding Author

Nicolas Delorme – Institut des Molécules et Matériaux du Mans (IMMM) – UMR CNRS 6283 – Le Mans Université, 72000 Le Mans, France; [orcid.org/0000-0003-4195-2000](https://orcid.org/0000-0003-4195-2000); Email: [nicolas.delorme@univ-lemans.fr](mailto:nicolas.delorme@univ-lemans.fr)

### Authors

David Siniscalco – Institut des Molécules et Matériaux du Mans (IMMM) – UMR CNRS 6283 – Le Mans Université, 72000 Le Mans, France; [orcid.org/0000-0002-2165-421X](https://orcid.org/0000-0002-2165-421X)

Laurence Pessoni – Bio-Inspired Materials Group: Functionalities & Self-Assembly, Université de Pau et des Pays de l'Adour, E2S UPPA, 64000 Pau, France; [orcid.org/0000-0001-9265-0091](https://orcid.org/0000-0001-9265-0091)

Laurent Billon – Bio-Inspired Materials Group: Functionalities & Self-Assembly, Université de Pau et des Pays de l'Adour, E2S UPPA, 64000 Pau, France; [orcid.org/0000-0003-0999-899X](https://orcid.org/0000-0003-0999-899X)

Anne Boussonnière – Institut des Molécules et Matériaux du Mans (IMMM) – UMR CNRS 6283 – Le Mans Université, 72000 Le Mans, France; [orcid.org/0000-0002-1113-099X](https://orcid.org/0000-0002-1113-099X)

Anne-Sophie Castanet – Institut des Molécules et Matériaux du Mans (IMMM) – UMR CNRS 6283 – Le Mans Université, 72000 Le Mans, France; [orcid.org/0000-0003-4704-4724](https://orcid.org/0000-0003-4704-4724)

Jean-François Bardeau – Institut des Molécules et Matériaux du Mans (IMMM) – UMR CNRS 6283 – Le Mans Université, 72000 Le Mans, France; [orcid.org/0000-0001-9240-3381](https://orcid.org/0000-0001-9240-3381)

Pierre Nickmilder – Laboratory for Physics of Nanomaterials and Energy (LPNE), Research Institute for Materials Science

and Engineering, University of Mons (UMONS), B 7000 Mons, Belgium

Philippe Leclère – Laboratory for Physics of Nanomaterials and Energy (LPNE), Research Institute for Materials Science and Engineering, University of Mons (UMONS), B 7000 Mons, Belgium; [orcid.org/0000-0002-5490-0608](https://orcid.org/0000-0002-5490-0608)

Complete contact information is available at:

<https://pubs.acs.org/10.1021/acsapm.3c01256>

## Funding

Agence Nationale pour la Recherche (ANR-20-CE06-0014-01); Région Pays de la Loire (Photoprint-PDL); AAC LUMOMAT ; F.R.S. – FNRS Grands Equipements (40007941) – 2022 “Interuniversity Platform for the Analysis of the Nanoscale Properties of Emerging Materials and Their Applications (ipanema)” ; F.R.S. – FNRS Projet de Recherche (PDR) (40007942) – 2022 “Piezoelectric and Flexoelectric Architectures from Hybrid Inorganic–Organic Nanomaterials—PiezoFlexoTronics”.

## Notes

The authors declare no competing financial interest.

## REFERENCES

- (1) Jerca, F. A.; Jerca, V. V.; Hoogenboom, R. Advances and opportunities in the exciting world of azobenzenes. *Nat. Rev. Chem.* **2022**, *6*, 51–69.
- (2) Wang, X. *Azo Polymers : Synthesis, Functions and Applications*; Springer-Verlag: Berlin Heidelberg, 2017; Vol. XIII, 15.
- (3) Zhao, R.; Mu, J.; Bai, J.; Zhao, W.; Gong, P.; Chen, L.; Zhang, N.; Shang, X.; Liu, F.; Yan, S. Smart Responsive Azo-Copolymer with Photoliquefaction for Switchable Adhesive Application. *ACS Appl. Mater. Interfaces* **2022**, *14*, 16678–16686.
- (4) Zhou, H.; Xue, C.; Weis, P.; Suzuki, Y.; Huang, S.; Koynov, K.; Auernhammer, G. K.; Berger, R.; Butt, H.-J.; Wu, S. Photoswitching of glass transition temperatures of azobenzene-containing polymers induces reversible solid-to-liquid transitions. *Nat. Chem.* **2017**, *9*, 145–151.
- (5) Zhang, P.; Cai, F.; Wang, W.; Wang, G.; Yu, H. Light-Switchable Adhesion of Azobenzene-Containing Siloxane-Based Tough Adhesive. *ACS Appl. Polym. Mater.* **2021**, *3*, 2325–2329.
- (6) Yang, B.; Cai, F.; Huang, S.; Yu, H. Athermal and Soft Multi-Nanopatterning of Azopolymers: Phototunable Mechanical Properties. *Angew. Chem., Int. Ed.* **2020**, *59*, 4035–4042.
- (7) Xu, W.-C.; Sun, S.; Wu, S. Photoinduced Reversible Solid-to-Liquid Transitions for Photoswitchable Materials. *Angew. Chem., Int. Ed.* **2019**, *58*, 9712–9740.
- (8) Koike, M.; Aizawa, M.; Akamatsu, N.; Shishido, A.; Matsuzawa, Y.; Yamamoto, T. Photoplasticization Behavior and Photoinduced Pressure-sensitive Adhesion Properties of Various Polymers containing an Azobenzene-doped Liquid Crystal. *Bull. Chem. Soc. Jpn.* **2020**, *93*, 1588.
- (9) Liang, S.; Li, S.; Yuan, C.; Zhang, D.; Chen, J.; Wu, S. Polyacrylate Backbone Promotes Photoinduced Reversible Solid-To-Liquid Transitions of Azobenzene-Containing Polymers. *Macromolecules* **2023**, *56*, 448–456.
- (10) Shang, C.; Xiong, Z.; Liu, S.; Yu, W. Molecular Dynamics of Azobenzene Polymer with Photoreversible Glass Transition. *Macromolecules* **2022**, *55*, 3711–3722.
- (11) Zhang, Z.; Chen, M.; Schneider, I.; Liu, Y.; Liang, S.; Sun, S.; Koynov, K.; Butt, H.-J.; Wu, S. Long Alkyl Side Chains Simultaneously Improve Mechanical Robustness and Healing Ability of a Photoswitchable Polymer. *Macromolecules* **2020**, *53*, 8562–8569.
- (12) Pessoni, L.; Siniscalco, D.; Boussonnière, A.; Castanet, A.-S.; Billon, L.; Delorme, N. Photo-reversible solid to liquid transition of azobenzene containing polymers: Impact of the chemical structure and chain length. *Eur. Polym. J.* **2022**, *174*, No. 111297.
- (13) Lakhera, N.; Graucob, A.; Schneider, A. S.; Kroner, E.; Arzt, E.; Yakacki, C. M.; Frick, C. P. Effect of viscoelasticity on the spherical and flat adhesion characteristics of photopolymerizable acrylate polymer networks. *Int. J. Adhes. Adhes.* **2013**, *44*, 184–194.
- (14) Delorme, N.; Chebil, M. S.; Vignaud, G.; Le Houerou, V.; Bardeau, J. F.; Busselez, R.; Gibaud, A.; Grohens, Y. Experimental evidence of ultrathin polymer film stratification by AFM force spectroscopy. *Eur. Phys. J. E: Soft Matter Biol. Phys.* **2015**, *38*, 56.
- (15) Lévy, R.; Maaloum, M. Measuring the spring constant of atomic force microscope cantilevers: thermal fluctuations and other methods. *Nanotechnology*. **2002**, *13*, 33–37.
- (16) Hermanowicz, P.; Sarna, M.; Burda, K.; Gabryś, H. AtomicJ: An open source software for analysis of force curves. *Rev. Sci. Instrum.* **2014**, *85*, No. 063703.
- (17) Pittenger, B.; Osechinskiy, S.; Yablon, D.; Mueller, T. Nanoscale DMA with the Atomic Force Microscope: A New Method for Measuring Viscoelastic Properties of Nanostructured Polymer Materials. *JOM* **2019**, *71*, 3390–3398.
- (18) Dokukin, M.; Sokolov, I. High-resolution high-speed dynamic mechanical spectroscopy of cells and other soft materials with the help of atomic force microscopy. *Sci. Rep.* **2015**, *5*, 12630.
- (19) Wool, R. P. Polymer entanglements. *Macromolecules* **1993**, *26*, 1564–1569.
- (20) Kim, K.-S.; Heo, J.-C.; Kim, K.-W. Effects of Temperature on the Microscale Adhesion Behavior of Thermoplastic Polymer Film. *Tribology Lett.* **2010**, *38*, 97–106.
- (21) O'Connor, A. E.; Willenbacher, N. The effect of molecular weight and temperature on tack properties of model polyisobutylenes. *Int. J. Adhes. Adhes.* **2004**, *24*, 335–346.
- (22) Mary, P.; Chateauinois, A.; Fretigny, C. Deformation of elastic coatings in adhesive contacts with spherical probes. *J. Phys. D: Appl. Phys.* **2006**, *39*, 3665.
- (23) Fox, T. G.; Loshaek, S. Influence of molecular weight and degree of crosslinking on the specific volume and glass temperature of polymers. *J. Polym. Sci.* **1955**, *15*, 371–390.
- (24) Pessoni, L.; Delorme, N.; Billon, L. Light-triggered surface properties of a glycolized PolyEthylene Terephthalate film by surface-initiated ATRP of azobenzene monomer. *Eur. Polym. J.* **2021**, *156*, No. 110608.